RSC Advances

PAPER

View Article Online
View Journal | View Issue

Cite this: *RSC Adv.*, 2017, **7**, 54235

Control of the molecular packing of chloroboron(III) and fluoroboron(III) subnaphthalocyanines by designing peripheral substituents†

Akuto Takagi and Tadashi Mizutani *

Chloroboron(III) and fluoroboron(III) hexa(1-alkynyl)- and hexa(2-arylethynyl)subnaphthalocyanines with a large dipole moment were prepared by Sonogashira coupling of hexaiodosubnaphthalocyanines with substituted acetylenes. Introduction of butyl or longer alkyl groups *via* ethynylene linkages on the periphery resulted in lower melting points and higher solubility in dichloromethane. X-ray diffraction (XRD) patterns of the cast film indicated that hexa(2-(4-hexylphenyl)ethynyl)- and hexa(2-(4-hexyloxyphenyl)ethynyl)subnaphthalocyanines with a B–F bond are packed in a discotic hexagonal columnar phase with lattice constants $a = 59–64$ Å and stacking distance $c = 4.7–4.8$ Å. The Q-band in visible spectra of the thin film of these B–F derivatives was blue-shifted, supporting the formation of H-aggregate in stacked columns. Polarized optical microscopy showed that these subnaphthalocyanines with a B–F bond exhibited a mesophase at 180 °C. XRD of these subnaphthalocyanines at 180 °C confirms a two dimensional hexagonal phase. XRD of the corresponding derivatives with a B–Cl bond showed that they were either amorphous or less crystalline. We suggest that the fluorine atom in the B–F group can fit into the cleft of cone-shaped subnaphthalocyanine, owing to the smaller van der Waals radius of F than Cl, to stabilize the columnar packing structure.

Received 9th October 2017
Accepted 21st November 2017

DOI: 10.1039/c7ra11104e

rsc.li/rsc-advances

Introduction

Cyclic oligopyrroles such as porphyrins and phthalocyanines are important dyes whose optical, redox, and semi-conductive properties have been employed in active materials for diverse optoelectric systems, such as photosynthesis, solar cells,[1] and electroluminescence devices.[2] Much effort has been directed toward the control of the molecular packing of these dyes,[3] which would affect the electrical conductivity of their films.[4] Charge carrier mobilities of phthalocyanines with eight alkoxy groups were reported to be dependent on the molecular packing, *i.e.*, crystalline, mesoscopic and isotropic phases.[5] Among cyclic oligopyrroles, subphthalocyanines have a unique cone shape,[6] and π-conjugation occurs on the cone-shaped framework.[7] Verreet *et al.*[8] reported that subnaphthalocyanine showed better energy conversion efficiency than subphthalocyanine in an organic solar cell combined with C_{60} due to the red shifted absorption. Subnaphthalocyanine with a larger core size than subphthalocyanine also has advantages as a semi-conductive material since Warman *et al.*[9] reported that the charge mobilities increase with increasing core sizes of the discotic molecules. In addition to the visible light absorption, redox properties, and semi-conductive properties, subphthalocyanines and subnaphthalocyanines have a large dipole moment nearly perpendicular to the π-conjugated electronic systems. Therefore, control of molecular packing would lead to unique dielectric functions that other cyclic oligo tetrapyrroles cannot exhibit. There have been several studies on the control of assembly of subphthalocyanines. Torres and co-workers reported that subphthalocyanines with nine dodecyloxy groups showed a liquid-crystalline phase which shows permanent polarization in the presence of electric fields.[10]

We have reported synthesis of subnaphthalocyanines with six halogen atoms on the naphthalene rings to tune the HOMO/LUMO energy levels as an active layer of photovoltaic cells.[12] Compared to subphthalocyanine, subnaphthalocyanine has a smaller HOMO–LUMO gap, and adsorbs visible light in the 600–700 nm range. Halogenation of subnaphthalocyanine resulted in a better orbital energy matching with fullerenes or fluorosubphthalocyanines at the p–n junction.[11] Introduction of six halogens in the periphery of subnaphthalocyanines cancelled the original dipole moment of subnaphthalocyanines because the dipole moment of a B–Cl bond and the combined dipole moment of C–halogen bonds are anti-parallel. As shown in Table 1, dipole moments of subnaphthalocyanines increases

Department of Molecular Chemistry and Biochemistry, Faculty of Science and Engineering, Doshisha University, Kyotanabe, Kyoto, 610-0321 Japan. E-mail: tmizutan@mail.doshisha.ac.jp

† Electronic supplementary information (ESI) available. See DOI: 10.1039/c7ra11104e

Table 1 Dipole moments of chloroboron(III) and fluoroboron(III) subnaphthalocyanines calculated with *ab initio* molecular orbital theory.[a] See Chart 1 for the structures

	Dipole moment/*D*	
Peripheral substituent (R)	X = Cl	X = F
Cl	1.51	0.22
F	2.61	1.08
I	3.78	2.76
H	5.24	3.91
PhC≡C–	6.32	4.88

[a] B3LYP/LAN2DZ for R = I, B3LYP/6-31G(D) for others.

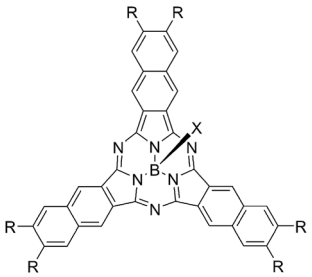

Chart 1 Structures of subnaphthalocyanines.

as the peripheral substituents are Cl < F < I < H < 2-phenylethynyl. Therefore, substitution of alkynyl groups on the naphthalene rings is an attractive strategy to obtain highly dipolar subnaphthalocyanines. The B–Cl derivatives showed a larger dipole moment than the B–F derivatives, but the B–Cl derivatives are more labile than the B–F derivatives. In this paper we report that hexaiodosubnaphthalocyanines were converted to hexa(1-alkynyl)subnaphthalocyanines and hexa(2-arylethynyl)subnaphthalocyanines, and changes in the peripheral substituents as well as the axial ligand from Cl to F can effectively control the molecular packing of these subnaphthalocyanine derivatives.

Results and discussion

Synthesis of chloroboron(III) and fluoroboron(III) hexa(1-alkynyl)subnaphthalocyanines and hexa(2-arylethynyl) subnaphthalocyanines

Chart 2 shows structures of subnaphthalocyanines studied in this paper. Synthetic routes to chloroboron(III) subnaphthalocyanines **1a–f** and fluoroboron(III) subnaphthalocyanines **2a–g** are shown in Scheme 1. Chloroboron(III) 3,4,12,13,21,22-hexaiodosubnaphthalocyanine was prepared according to the literature.[12,13] Bender and coworkers reported that cyclotrimerization of unsubstituted 2,3-naphthalenedicarbonitrile in the presence of BCl_3 gave by-products with naphthalene rings chlorinated,[14] while cyclotrimerization of 6,7-diiodo-2,3-naphthalenedicarbonitrile **11** did not give any chlorinated by-products owing to the inactivation of naphthalene ring toward electrophilic substitution by iodine groups. Therefore, isolation

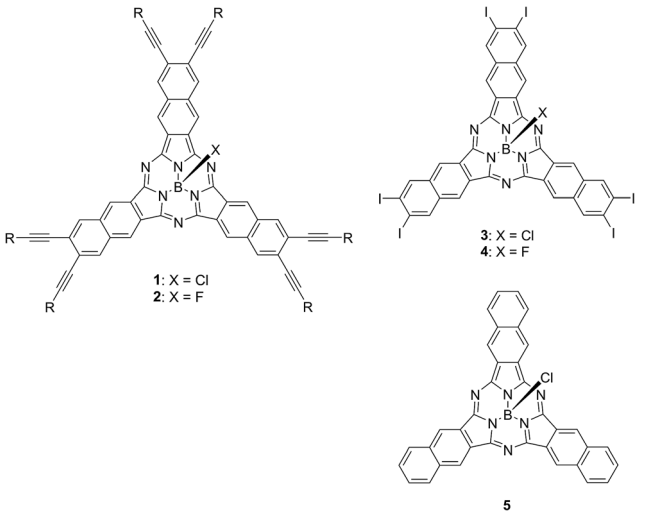

Chart 2 Structures of subnaphthalocyanines **1–5**.

of **3** was facile. Sonogashira coupling was employed to substitute iodines of hexaiodosubnaphthalocyanine **3** with alkynyl groups.[15] B–Cl derivatives **1a–f** were isolated with silica gel column chromatography eluted with toluene.

Substitution of axial Cl with F by Torres's procedure[16] gave fluoroboron(III) 3,4,12,13,21,22-hexaiodosubnaphthalocyanine **4**. B–F derivatives **2a–g** were prepared similarly from fluoroboron(III) hexaiodosubnaphthalocyanine **4** by Sonogashira coupling, and isolated using silica gel column chromatography, except for **2c**. For **2c**, owing to low solubility in organic solvents, the product was crystallized by adding hexane to the reaction mixture, and the crystal was washed with organic solvents, and dried *in vacuo*. The precursor **15**, a coupling component for **2g**, was prepared according to the literature (Scheme 2).[17] These subnaphthalocyanines were identified by ^{1}H NMR, ^{13}C NMR,

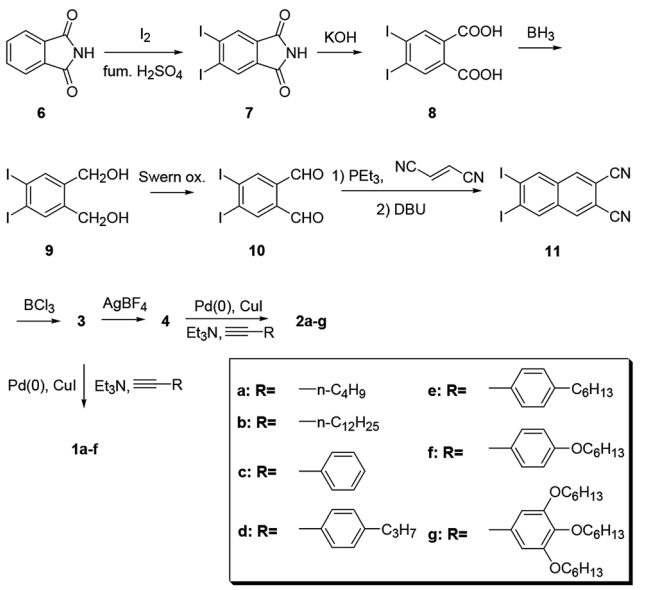

Scheme 1 Synthesis of substituted subnaphthalocyanines **1** and **2**.

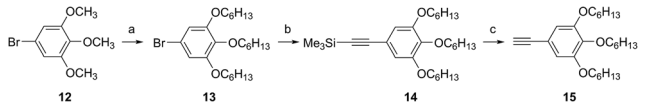

Scheme 2 Synthesis of arylethyne **15**. Reagents and conditions. (a) BBr_3; $C_6H_{13}Br$, K_2CO_3, 65%; (b) trimethylsilylacetylene, $Pd(PPh_3)_4$–CuI, piperidine, 80 °C, 98%; (c) K_2CO_3, DCM/MeOH, 86%.

MALDI-TOF mass spectroscopy, high resolution FAB mass spectroscopy and UV-visible spectroscopy. Their purities were checked by gel-permeation HPLC, which clearly detected the presence of penta- or tetrasubstituted by-products before silica gel column purification. Isolated yields of Sonogashira coupling are listed in Table 2. The yields of Sonogashira coupling were 3–8% for B–Cl derivatives **1**, while they were 10–27% for B–F derivatives **2**. Lower yields of B–Cl derivatives **1** can be ascribed to the labile B–Cl bond. The B–F derivatives **2** were also prepared from the B–Cl derivatives **1** by substitution of Cl with F, but the overall yields were lower in this route, due to the labile B–Cl bond.

Solubilities and melting points

Solubilities and melting points of subnaphthalocyanines **1a–f** and **2a–g** are listed in Table 3. Solubilities were determined by measuring the absorbances of saturated solutions with UV-visible spectrophotometry. The molar extinction coefficients at the Q-band peak were determined using 2×10^{-6} M CH_2Cl_2 solutions. Compared to unsubstituted chloroboron(III) subnaphthalocyanine **5**, **1a–f** were 40 to 310 times more soluble in CH_2Cl_2. Solubilities increased with longer alkyl groups for homologs **1a**/**1b** and **1c**/**1d**/**1e**. By substitution of axial Cl with F, solubilities were much lower, showing that a smaller fluorine atom would stabilize molecular packing in the solid state. This observation is contrary to the previous report that fluoroboron(III) subphthalocyanine showed higher solubility than chloroboron(III) subphthalocyanine and bromoboron(III) subphthalocyanine.[18] Melting points of 1-alkynyl derivatives **2a** and **2b** were lower than 120 °C, while those of 2-phenylethynyl and 2-(4-propylphenyl)ethynyl derivative (**2c** and **2d**) were higher than 375 °C. Thus, melting points were lowered by introduction of alkyl groups in the periphery, and raised by introduction of phenyl groups. Polarized optical microscope (POM) observation under cross-Nicole conditions displayed that the thin film of chloroboron(III) derivatives **1a–f** were optically isotropic in the solid state, indicating that these are in a glassy state. Therefore, the temperatures reported for **1a–f** listed in Table 3 are glass transition temperatures. For fluoroboron(III) derivatives **2a–f**, the thin film was crystalline, as confirmed by the bright image observed with a POM under cross-Nicole conditions. The thin film of **2g** was not crystalline as judged by POM observations.

Table 2 Yields of Sonogashira coupling to afford subnaphthalocyanines **1a–f** and **2a–g**

	Yield (%)		Yield (%)
1a	7	**2a**	19
1b	6	**2b**	16
1c	8	**2c**	10
1d	8	**2d**	20
1e	6	**2e**	22
1f	3	**2f**	27
		2g	10

Table 3 Solubilities of subnaphthalocyanines **1a–f**, **2a–g** and **5** in dichloromethane at 25 °C and melting points or glass transition temperatures

	Solubility (g L^{-1})	Melting point or glass transition temperature (°C)
1a	5.02	77–80[a]
1b	9.37	70–73[a]
1c	1.19	>375
1d	1.52	>375
1e	2.13	102–108[a]
1f	3.70	98–106[a]
2a	1.35	114–118
2b	2.30	100–105
2c	6.48×10^{-4}	>375
2d	0.90	>375
2e	1.62	170–178
2f	2.01	168–176
2g	10.62	80–86[a]
5	0.03	270–276

[a] Glass transition temperature.

UV-visible spectra in solutions and of cast films

Chloroboron(III) subnaphthalocyanine **5** in toluene shows a strong absorption at 660 nm and an absorption at 299 nm in the near UV with almost equal absorbances.[19] The former band is called a Q-band, and the latter band is called a B-band or a Soret band. Fig. 1 shows UV-visible spectra of B–Cl derivatives **1** in CH_2Cl_2. The absorption maxima in the Q-band were shifted to the longer wavelength in the order: **5** (H) < **1a**, **b** (1-alkynyl) < **1c–f** (2-arylethynyl). The molar absorption coefficients of **1a–f**

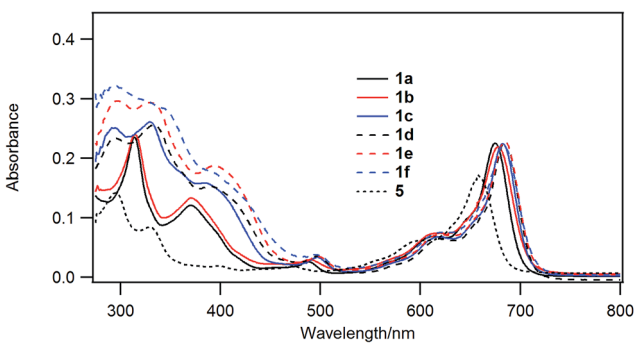

Fig. 1 UV-visible spectra of **1a** (black solid line), **1b** (red solid line), **1c** (blue solid line), **1d** (black dashed line), **1e** (red dashed line), and **1f** (blue dashed line) and the parent chloroboron(III) subnaphthalocyanine **5** (black dotted line). The concentration was 2×10^{-6} M in dichloromethane.

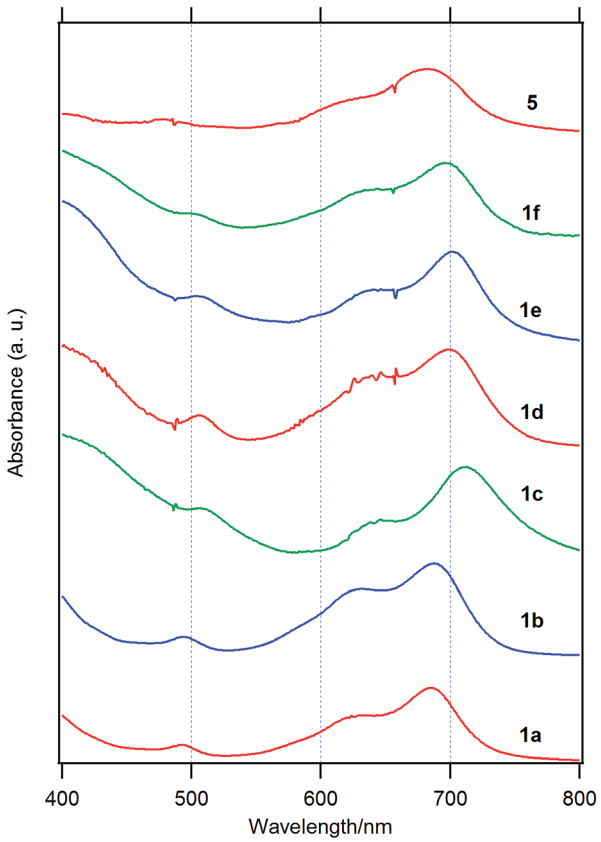

Fig. 2 Visible spectra of **1a**, **1b**, **1c**, **1d**, **1e**, and **1f** and the parent chloroboron(III) subnaphthalocyanine **5** on silicate glass.

were larger than that of the parent **5**. The substituent effects are more obvious in the B-band in the 300–500 nm region: **1a** and **1b** with 1-alkynyl groups showed peaks at 318 and 369 nm, while **1c–f** with 2-arylethynyl groups showed a more intense absorption in the B-band. Fig. 2 shows the visible spectra of B–Cl derivatives of the cast film on silicate glass. A solution of **1** in dichloromethane was dropped on silicate glass, and the film was kept at room temperature in Ar for 2 days. The absorption maxima in the Q-band were shifted to the longer wavelength in the order: **5** (H) < **1a, 1b** (1-alkynyl) < **1d–f** (4-alkyl or 4-alkoxyphenylethynyl) < **1c** (phenyl).

Table 4 Absorption maxima in the Q-band of **1a–f** and reference subnaphthalocyanine **5** in dichloromethane, on silicate glass, and these shift

	λ_{abs} (nm)		
	In CH_2Cl_2	On silicate glass	Shift
1a	675	685	10
1b	678	687	9
1c	682	712	30
1d	685	698	13
1e	685	703	18
1f	683	696	13
5	658	680	22

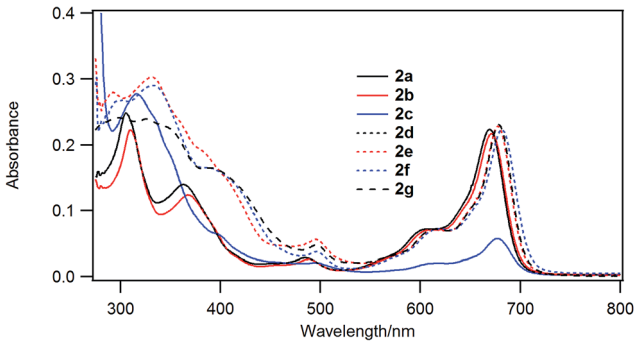

Fig. 3 UV-visible spectra of **2a** (black solid line), **2b** (red solid line), **2c** (blue solid line), **2d** (black dotted line), **2e** (red dotted line), **2f** (blue dotted line), and **2g** (black dashed line). The concentration of **2a**, **2b** and **2d–g** was 2×10^{-6} M in dichloromethane. Visible spectra of **2c** was the spectra of saturated dichloromethane solution.

In Table 4 are listed the absorption maxima in solution and of the cast film. The shifts of the Q-band of B–Cl derivatives of the cast film to the longer wavelength compared to that in solutions indicate that J-aggregate forms in the cast film. The displacements are 9–30 nm, and increased in the order: **1a, 1b** (alkyl) < **1d–f** (alkylphenyl or alkoxyphenyl) < **5** (H) < **1c** (phenyl).

Fig. 3 shows the UV-visible spectra of the B–F derivatives **2** in CH_2Cl_2. The absorption maxima were shifted to the longer wavelength in the order: **2a, b** (alkyl) < **2c–f** (phenyl) in CH_2Cl_2.

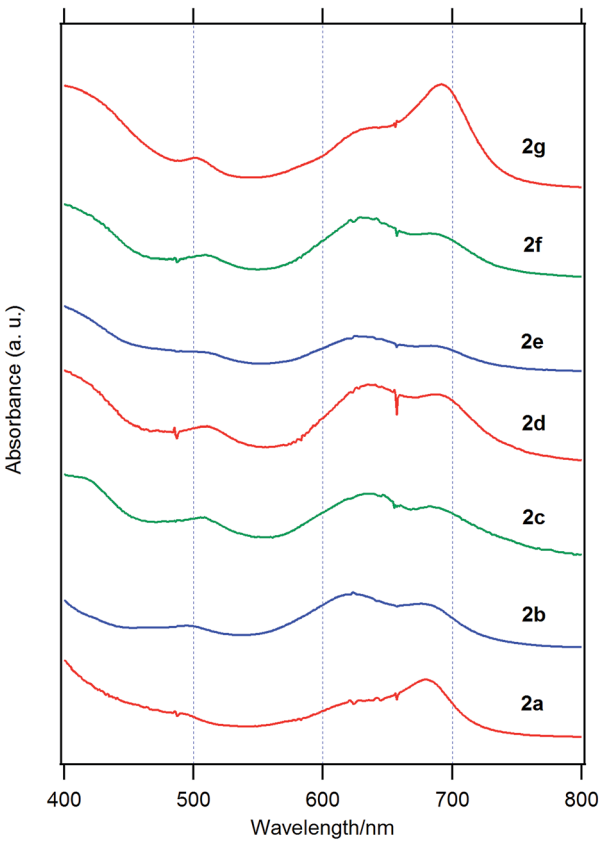

Fig. 4 Visible spectra of **2a**, **2b**, **2c**, **2d**, **2e**, **2f**, and **2g** on silicate glass.

Table 5 Absorption maxima in the Q-band of **2a–g** in CH_2Cl_2, on silicate glass, and these shift

	λ_{abs} (nm)		
	In CH_2Cl_2	On silicate glass	Shift
2a	669	679	10
2b	671	624	−47
2c	677	632	−45
2d	678	642	−36
2e	678	625	−53
2f	681	629	−52
2g	678	692	14

The B-band was also affected by substituents in a similar way as the B–Cl derivatives. The molar absorption coefficients of all of alkynyl substituted derivatives were similar. Fig. 4 shows visible spectra of B–F derivatives **2** of the cast film on silicate glass. Solutions of **2a–b** and **2d–g** in dichloromethane and **2c** in pyridine were dropped on silicate glass, the solvent was evaporated, and the resulting film was kept in Ar for 2 days before recording visible spectra. The spectra were almost identical with those of as-prepared film. In Table 5 are listed the absorption maxima in solution and of the cast film. It is noteworthy that the Q-band absorption envelope of **2b–f** is different from that in CH_2Cl_2, that of **1** in CH_2Cl_2, and that of **1** of the cast film. The Q-band of **2b–f** of the cast film exhibited larger absorption in the 600–650 nm range than the absorption band in the 650–700 nm range. The shifts to the shorter wavelength indicate that **2b–f** form H-aggregate in the cast film.[20] Phthalocyanines with oligo(ethylene oxide) units showed a blue-shifted Q-band, and it was ascribed to formation of H-aggregate.[21] The Q-band spectral shapes are similar to those reported for μ-oxo dimers of iron phthalocyanines[22,23] and subphthalocyanines,[24] supporting the formation of a stacked dimer or a stacked column in the cast film. In contrast, the Q-band of **2a** and **2g** of the cast film was similar to those observed for B–Cl derivatives **1**: 10–14 nm red-shift relative to the peak maximum in solution indicated that **2a** and **2g** do not form H-aggregate in the cast film.

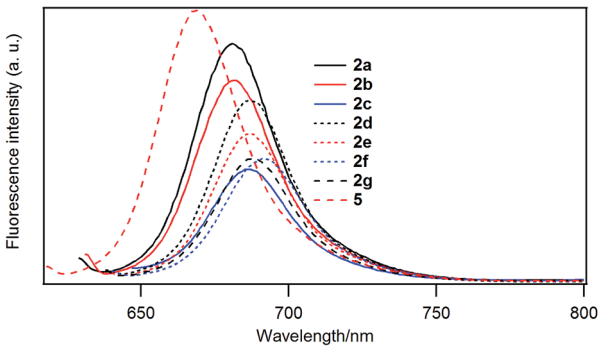

Fig. 5 Fluorescence spectra of **2a** (black solid line), **2b** (red solid line), **2c** (blue solid line), **2d** (black dotted line), **2e** (red dotted line), **2f** (blue dotted line), and **2g** (black dashed line), and **5** (red dashed line) at 298 K in dichloromethane where the samples were excited at (λ_{max} abs − 50) nm. Each sample has absorbance of 0.02 at the excitation wavelength.

Table 6 Absorption and emission maxima, and fluorescence quantum yields of **2a–g** and reference subnaphthalocyanine **5** in CH_2Cl_2

	λ_{abs}/nm	λ_{em}/nm	Stokes shift (nm)	Fluorescence quantum yield
2a	669	681	12	0.19
2b	671	682	11	0.16
2c	677	687	10	0.09
2d	678	687	9	0.14
2e	678	686	8	0.11
2f	680	691	11	0.10
2g	678	688	10	0.10
5	658	669	11	0.22

Fluorescence spectra

Fig. 5 shows the fluorescence emission spectra of the B–F derivatives in CH_2Cl_2. In Table 6 are listed the emission maxima, Stokes shifts, and fluorescence quantum yields. The fluorescence quantum yields were determined based on the reported quantum yield of unsubstituted derivative **5** (0.22).[25] The fluorescence quantum yields decreased in the order: **5** (H) > **2a** ($-C_4H_9$) > **2b** ($-C_{12}H_{25}$) > **2d** ($-PhC_3H_7$) > **2e** ($-PhC_6H_{13}$) > **2f** ($-PhOC_6H_{13}$), **2g** ($-Ph(OC_6H_{13})_3$) > **2c** (–Ph).

Fluorescence emission spectra of **2b**, **2d**, **2e** and **2f** in CH_2Cl_2 : DMSO (1 : 1, v/v) are shown in Fig. S51.† In addition to the emission band peaked at 685–689 nm, **2b** and **2e** exhibited a new band around 800 nm. Excitation spectra for the new band are shown in Fig. S52 and S53,† and they were similar to the UV-visible spectra of the thin film shown in Fig. 4. Therefore, **2b** and **2e** form H-aggregate in CH_2Cl_2–DMSO (1 : 1), whose structures are similar to those formed in the cast film.

Polarized optical microscope

Fig. 6 shows the polarized optical microscopic images of the cast film of **2e** and **2f** under crossed-Nicols conditions at 180 °C above the melting point. The film was sandwiched between two glasses and the glasses were pressed above the melting point. These images clearly showed that these films are optically anisotropic above the melting point. We also attempted to

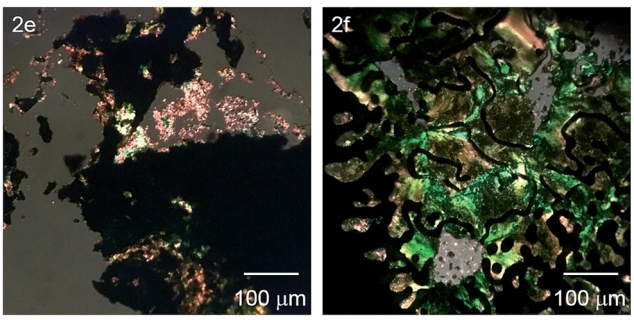

Fig. 6 POM microphotographs of **2e** and **2f** at 180 °C under crossed-Nicols conditions.

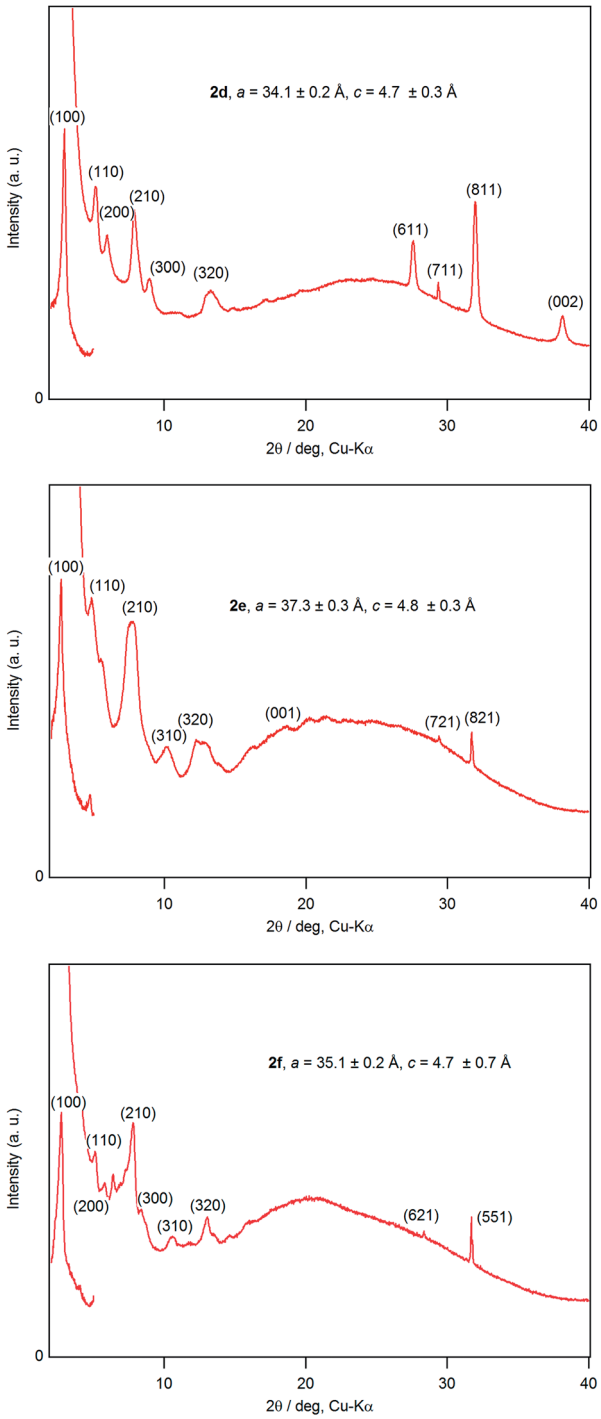

Fig. 7 Powder X-ray diffraction patterns of **2d–f**. Lattice constants, a and c, were determined by least-squares fitting based on the hexagonal lattice: $\frac{1}{d} = \sqrt{\frac{4}{3}\frac{h^2 + hk + k^2}{a^2} + \frac{l^2}{c^2}}$. While the XRD patterns were recorded with a 1D silicon strip detector for a wide angle region, $2\theta > 3°$, they were recorded with a 0D detector for the low angle region, $2\theta = 2–5°$.

detect phase transition by differential scanning calorimetry, while no clear enthalpy changes were observed. Slow kinetics due to highly viscous nature and/or low degree of crystallinity may be responsible for the lack of DSC peaks. Serrano and coworkers reported that no DSC peak was observed for the liquid crystalline porphyrin derivatives.[26]

Table 7 Powder X-ray diffraction peaks of **2d**, d-spacings, and Miller indices (hkl) based on the hexagonal lattice with $a = 34.1 \pm 0.2$ Å and $c = 4.7 \pm 0.3$ Å

2θ (deg)	d (Å)	(hkl)	2θ (deg)	d (Å)	(hkl)
2.95	29.88	(100)	13.19	6.71	(320)
5.32	16.59	(110)	27.54	3.24	(611)
6.08	14.52	(200)	29.34	3.04	(711)
7.84	11.27	(210)	31.93	2.80	(811)
8.95	9.87	(300)	38.10	2.36	(002)

Powder X-ray diffraction

A dichloromethane solution of **2d**, **2e**, and **2f** was dropped on silicate glass, and the glass plate was dried at room temperature for 2 weeks in dark in Ar to allow crystallization. A thin film of **2d**, **2e**, and **2f** prepared in this way was subjected to powder X-ray diffraction studies (Fig. 7). All films showed a diffraction peak in the low angle region around 2θ of 2.8°, showing a long distance periodicity. The diffraction peaks were indexed based on a two-dimensional hexagonal lattice as shown in Tables 7–9. The hexagonal lattice parameter a ranged from 34.1 to 37.3 Å. We also assigned some of the peaks to the stacking distance along the c direction. It should be noted that the peaks originating from the stacking distance at $2\theta = 29.45°$ and 31.69° for **2e** as well as the peaks at 28.34° and 31.70° for **2f** were not observed for the as-prepared cast film before aging. This observation suggests that the hexagonal column are formed quickly, while the periodic stacking of the cone-shaped molecules occurs slowly. The lattice constant c ranged from 4.7 to 4.8 Å. These X-ray diffraction studies confirm the hexagonal columnar structure of fluoroboron(III) subnaphthalocyanines bearing 2-(4-alkylphenyl)ethynyl groups in the cast film. In contrast to the B–F derivatives, XRD of B–Cl derivatives **1d**, **1e**, and **1f** indicates that they are poorly crystalline (see Fig. S78–S80 in ESI†). Clays, Kim and coworkers[27] reported that hexakis(hexadecylthio)subphthalocyanine exhibited hexagonal columnar mesophase with a lattice constant $a = 33.02$ Å. The molecular size of this compound is similar to **2f**, if the alkyl chains adopt anti conformer. Torres and coworkers reported that dodecafluorosubphthalocyanine with a B–F bond formed a one-dimensional column in the crystal, where the B–B distance, *i.e.*, the stacking distance, was 4.5 Å.[28]

Table 8 Powder X-ray diffraction peaks of **2e**, d-spacings and Miller indices (hkl) based on the hexagonal lattice with $a = 37.3 \pm 0.3$ Å and $c = 4.8 \pm 0.3$ Å

2θ (deg)	d (Å)	(hkl)	2θ (deg)	d (Å)	(hkl)
2.70	32.65	(100)	13.02	6.79	(410)
4.84	18.24	(110)	18.41	4.82	(001)
7.52	11.75	(210)	29.45	3.03	(721)
7.83	11.28	(300)	31.69	2.82	(821)
10.13	8.73	(310)	42.62	2.12	(622)
12.22	7.23	(320)			

Table 9 Powder X-ray diffraction peaks of **2f**, *d*-spacings, and Miller indices (*hkl*) based on the hexagonal lattice with $a = 35.1 \pm 0.2$ Å and $c = 4.7 \pm 0.7$ Å

2θ (deg)	*d* (Å)	(*hkl*)	2θ (deg)	*d* (Å)	(*hkl*)
2.90	30.45	(100)	10.51	8.41	(310)
5.10	17.31	(110)	12.98	6.81	(320)
5.78	15.28	(200)	28.34	3.15	(621)
7.81	11.31	(210)	31.70	2.82	(551)
8.26	10.70	(300)			

Fig. 8 shows XRD patterns of films of **2e** and **2f** at 25 °C and 180 °C. Diffraction peaks owing to two dimensional hexagonal lattice (*hk*0) appeared at 180 °C, indicating that the films retain the hexagonal columnar structure at 180 °C. The diffraction peaks in the range 28–32° due to the stacking ordering along the *c*-axis direction disappeared at 180 °C. Combined with the POM observations described above, **2e** and **2f** were in a discotic hexagonal columnar mesophase at 180 °C.

Molecular orbital calculations of the stacked dimer of 1c and 2c

The energy of stacked dimers of **1c** and **2c** relative to monomeric **1c** and **2c** was calculated at the B3LYP/6-31G(D) level with a fixed

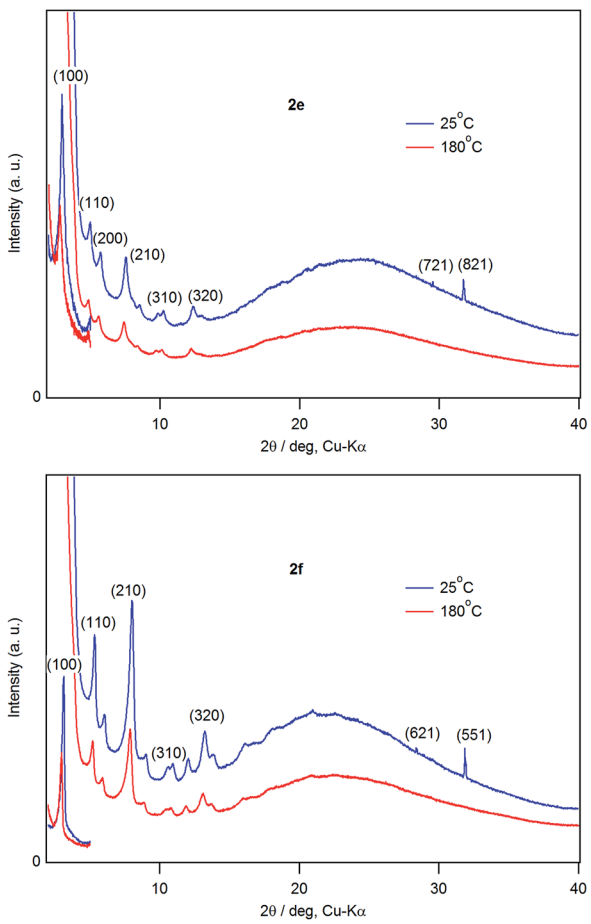

Fig. 8 Variable-temperature XRD of **2e** and **2f**.

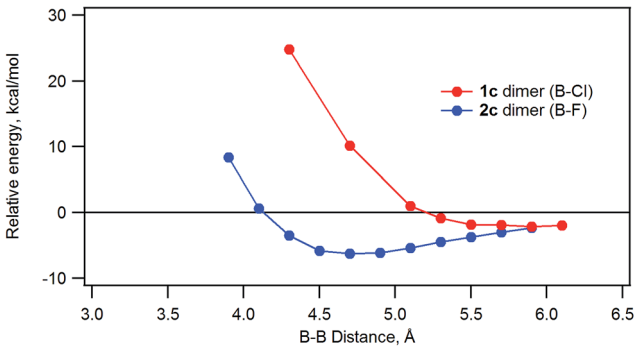

Fig. 9 Plot of the relative energy of dimeric **1c** or **2c** against the B–B distance calculated by *ab initio* B3LYP/6-31G(D).

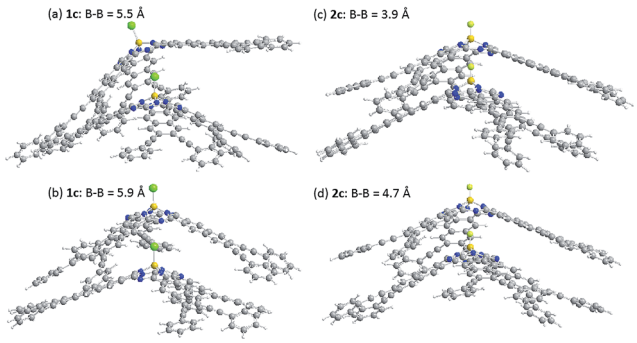

Fig. 10 Optimized structures of dimeric subnaphthalocyanines **1c** and **2c**. (a) **1c**, B–B distance of 5.5 Å, (b) **1c**, B–B distance of 5.9 Å, (c) **2c**, B–B distance of 3.9 Å, and (d) **2c**, B–B distance of 4.7 Å.

distance between the two B atoms of the dimer. The energies were plotted against the B–B distance in Fig. 9. The energy of the dimeric B–Cl derivative **1c** decreased as the B–B distance was longer, while the energy of the dimeric B–F derivative **2c** showed a minimum at about 4.7 Å of the B–B distance. The geometry optimized structures are shown in Fig. 10. At the B–B distance of 5.5 Å, the dimeric **1c** showed a bent structure due to a large van der Waals radius of Cl, while the dimeric **2c** showed a linear structure even at a B–B distance of 3.9 Å. The van der Waals radii of B,[29] C, F, and Cl[30] are 1.92, 1.7, 1.47, and 1.75 Å. Therefore, sum of the van der Waals radii, B + F, are shorter than that of C + C, while sum of the van der Waals radii, B + Cl, are larger than that of C + C. These molecular modelling studies indicate that the smaller van der Waals radius of F atom can fit to the cleft of cone-shaped subnaphthalocyanine and lead to a stable stacked structure.

Experimental

^{1}H and ^{13}C nuclear magnetic resonance (NMR) spectra were recorded on a JEOL JNM-ECX DELTA spectrometer using tetramethylsilane as an internal reference (0 ppm). Matrix-assisted laser desorption/ionization time-of-flight (MALDI-TOF) mass spectra were obtained with a Brucker Autoflex Speed mass spectrometer. High resolution FAB MS spectra were recorded

with a JEOL JMS-700 MStation. Gel-permeation HPLC was performed with a Shimadzu liquid chromatography LC-6AD using Tosoh TSKgel G2000H as a stationary phase and chloroform as eluant. Powder X-ray diffraction was recorded with a Rigaku SmartLab diffractometer with Cu-Kα radiation. The low angle region, 2θ of 2 to 5°, was recorded with the 0D detector, while the wide angle region, 2θ of 3 to 40°, was recorded with the 1D silicon strip detector. Variable temperature XRD was recorded for a thin film of subnaphthalocyanines on silicate glass placed in a thermostated Pt holder. Melting points were determined by observing changes in the sample sandwiched between two glasses heated at a rate of 2 °C min on Mettler-Toredo FP82HT hot stage with a polarized optical microscope Nikon Eclipse LV100 POL. Molecular orbital calculations were performed with Gaussian 09.[31]

Synthesis of subnaphthalocyanines

1a. In a 100 mL three-necked flask were placed **3** (68 mg, 0.051 mmol), copper iodide (10 mg, 0.053 mmol), $Pd(PPh_3)_4$ (30 mg, 0.026 mmol), dry toluene (30 mL), and triethylamine (5.0 mL). 1-Hexyne (1.43 g, 17.4 mmol) was added and the mixture was stirred at 40 °C under Ar for 20 h. The reaction was quenched by the addition of water and the organic layer was separated. The aqueous layer was washed with dichloromethane three times and the dichloromethane solution was combined with the organic layer. The organic solvent was evaporated and the residue was subjected to silica gel column chromatography using toluene to obtain 3.8 mg (7%) of **1a**.

^{1}H-NMR ($CDCl_3$, 500 MHz): δ (ppm) = 9.25 (s, 6H), 8.36 (s, 6H), 2.58 (t, 12H), 1.76–1.66 (m, 12H), 1.65–1.57 (m, 12H), 1.02 (t, 18H). ^{13}C-NMR ($CDCl_3$, 125 MHz): δ (ppm) 148.74, 132.97, 131.94, 128.88, 124.98, 121.64, 95.97, 79.61, 30.87, 22.11, 19.57, 13.77. MALDI-TOF mass: m/z = 1061.3 [$(M + H)^+$], calcd for $C_{72}H_{67}BN_6Cl$ m/z = 1061.5. HRMS (FAB): m/z = 1060.5144, calcd for $^{12}C_{72}{}^1H_{66}{}^{14}N_6{}^{35}Cl$ ^{11}B m/z = 1060.5131. Visible (dichloromethane) λ_{max}/nm (log ε): 675 (5.05).

1b. In a 100 mL three-necked flask were placed **3** (68 mg, 0.051 mmol), copper iodide (10 mg, 0.053 mmol), $Pd(PPh_3)_4$ (30 mg, 0.026 mmol), dry toluene (30 mL), and triethylamine (5.0 mL). 1-Tetradecyne (800 mg, 4.12 mmol) was added and the mixture was stirred at 40 °C under Ar for 20 h. The reaction was quenched by the addition of water and the organic layer was separated. The aqueous layer was washed with dichloromethane three times and the dichloromethane solution was combined with the organic layer. The organic solvent was evaporated and the residue was subjected to silica gel column chromatography using toluene to obtain 5.3 mg (6%) of **1b**.

^{1}H-NMR ($CDCl_3$, 500 MHz): δ (ppm) = 9.26 (s, 6H), 8.35 (s, 6H), 2.57 (t, 12H), 1.74–1.70 (m, 12H), 1.42–1.22 (m, 108H), 0.88 (t, 18H). ^{13}C-NMR ($CDCl_3$, 125 MHz): δ (ppm) 148.86, 132.94, 131.96, 128.93, 125.05, 121.66, 96.11, 79.57, 31.95, 29.75, 29.71, 29.66, 29.40, 29.35, 29.10, 28.87, 22.71, 19.91, 14.14. MALDI-TOF mass: m/z = 1734.4 [$(M + H)^+$], calcd for $C_{120}H_{163}BN_6Cl$ m/z = 1734.3. Visible (dichloromethane) λ_{max}/nm (log ε): 678 (5.04).

1c. In a 100 mL three-necked flask were placed **3** (68 mg, 0.051 mmol), copper iodide (10 mg, 0.053 mmol), $Pd(PPh_3)_4$ (30 mg, 0.026 mmol), dry toluene (30 mL), and triethylamine (5.0 mL). Ethynylbenzene (310 mg, 3.03 mmol) was added and the mixture was stirred at 40 °C under Ar for 20 h. The reaction was quenched by the addition of water and the organic layer was separated. The aqueous layer was washed with dichloromethane three times and the dichloromethane solution was combined with the organic layer. The organic solvent was evaporated and the residue was subjected to silica gel column chromatography using toluene to obtain 4.8 mg (8%) of **1c**.

^{1}H-NMR ($CDCl_3$, 500 MHz): δ (ppm) = 9.25 (s, 6H), 8.51 (s, 6H), 7.73–7.60 (m, 12H), 7.45–7.33 (m, 18H). MALDI-TOF mass: m/z = 1181.2 [$(M + H)^+$], calcd for $C_{84}H_{43}BN_6Cl$ m/z = 1181.3. HRMS (FAB): m/z = 1180.3259, calcd for $^{12}C_{84}{}^1H_{42}{}^{14}N_6{}^{35}Cl$ ^{11}B m/z = 1180.3253. Visible (dichloromethane) λ_{max}/nm (log ε): 682 (5.05).

1d. In a 100 mL three-necked flask were placed **3** (68 mg, 0.051 mmol), copper iodide (10 mg, 0.053 mmol), $Pd(PPh_3)_4$ (30 mg, 0.026 mmol), dry toluene (30 mL), and triethylamine (5.0 mL). 1-Ethynyl-3-propylbenzene (440 mg, 3.05 mmol) was added and the mixture was stirred at 40 °C under Ar for 20 h. The reaction was quenched by the addition of water and the organic layer was separated. The aqueous layer was washed with dichloromethane three times and the dichloromethane solution was combined with the organic layer. The organic solvent was evaporated and subjected to silica gel column chromatography using toluene to obtain 5.8 mg (8%) of **1d**.

^{1}H-NMR ($CDCl_3$, 500 MHz): δ (ppm) = 9.25 (s, 6H), 8.49 (s, 6H), 7.58 (d, 12H, 5 Hz), 7.21 (d, 12H, 5 Hz), 2.64 (t, 12H), 1.72–1.65 (m, 12H), 0.98 (t, 18H). MALDI-TOF mass: m/z = 1432.8 [M^+], calcd for $C_{102}H_{78}BN_6Cl$ m/z = 1432.6. Visible (dichloromethane) λ_{max}/nm (log ε): 685 (5.06).

1e. In a 100 mL three-necked flask were placed **3** (68 mg, 0.051 mmol), copper iodide (10 mg, 0.053 mmol), $Pd(PPh_3)_4$ (30 mg, 0.026 mmol), dry toluene (30 mL), and triethylamine (5.0 mL). *p*-Ethynylhexylbenzene (570 mg, 3.06 mmol) was added and the mixture was stirred at 40 °C under Ar for 20 h. The reaction was quenched by the addition of water and the organic layer was separated. The aqueous layer was washed with dichloromethane three times and the dichloromethane solution was combined with the organic layer. The organic solvent was evaporated and the residue was subjected to silica gel column chromatography using toluene to obtain 5.1 mg (6%) of **1e**.

^{1}H-NMR ($CDCl_3$, 500 MHz): δ (ppm) = 9.26 (s, 6H), 8.50 (s, 6H), 7.58 (d, 12H, 5 Hz), 7.21 (d, 12H, 5 Hz), 2.66 (t, 12H), 1.66–1.62 (m, 12H), 1.40–1.29 (m, 36H), 0.91 (t, 18H). MALDI-TOF mass: m/z = 1686.1 [$(M + H)^+$], calcd for $C_{120}H_{115}BN_6Cl$ m/z = 1685.9. Visible (dichloromethane) λ_{max}/nm (log ε): 685 (5.06).

1f. In a 100 mL three-necked flask were placed **3** (68 mg, 0.051 mmol), copper iodide (10 mg, 0.053 mmol), $Pd(PPh_3)_4$ (30 mg, 0.026 mmol), dry toluene (30 mL), and triethylamine (5.0 mL). *p*-Ethynyl(hexyloxy)benzene (620 mg, 3.06 mmol) was added and the mixture was stirred at 40 °C under Ar for 20 h. The reaction was quenched by the addition of water and the organic layer was separated. The aqueous layer was washed with dichloromethane three times and the dichloromethane solution was combined with the organic layer. The organic solvent

was evaporated and the residue was subjected to silica gel column chromatography using toluene to obtain 2.7 mg (3%) of **1f**.

^{1}H-NMR ($CDCl_3$, 500 MHz): δ (ppm) = 9.29 (s, 6H), 8.49 (s, 6H), 7.59 (d, 12H, 10 Hz), 6.92 (d, 12H, 10 Hz), 4.01 (t, 12H), 1.84–1.79 (m, 12H), 1.51–1.47 (m, 12H), 1.42–1.32 (m, 24H), 0.93 (t, 18H). MALDI-TOF mass: m/z = 1781.1 [M^+], calcd for $C_{120}H_{114}BN_6O_6Cl$ m/z = 1780.9. Visible (dichloromethane) λ_{max}/nm (log ε): 683 (5.04).

2a. In a 100 mL three-necked flask were placed **4** (68 mg, 0.052 mmol), copper iodide (10 mg, 0.053 mmol), $Pd(PPh_3)_4$ (30 mg, 0.026 mmol), dry dimethylsulfoxide (30 mL), and triethylamine (5.0 mL). 1-Hexyne (1.40 g, 17.0 mmol) was added and the mixture was stirred at 40 °C under Ar for 20 h. The reaction was quenched by the addition of water. This solution was washed with dichloromethane three times. The organic solvent was evaporated and the residual oil containing a small amount of DMSO was subjected to silica gel column chromatography using toluene to obtain 10.1 mg (19%) of **2a**.

^{1}H-NMR ($CDCl_3$, 500 MHz): δ (ppm) = 9.22 (s, 6H), 8.34 (s, 6H), 2.58 (t, 12H), 1.73–1.68 (m, 12H), 1.63–1.58 (m, 12H), 1.01 (t, 18H). MALDI-TOF mass: m/z = 1044.7 [M^+], calcd for $C_{72}H_{66}BN_6F$ m/z = 1044.5. HRMS (FAB): m/z = 1044.5413, calcd for $^{12}C_{72}{}^1H_{66}{}^{14}N_6{}^{19}F$ ^{11}B m/z = 1044.5426. Visible (dichloromethane) λ_{max}/nm (log ε): 669 (5.05).

2b. In a 100 mL three-necked flask were placed **4** (68 mg, 0.052 mmol), copper iodide (10 mg, 0.053 mmol), $Pd(PPh_3)_4$ (30 mg, 0.026 mmol), and dry dimethylsulfoxide (30 mL), and triethylamine (5.0 mL). 1-Tetradecyne (600 mg, 3.08 mmol) was added and the mixture was stirred at 40 °C under Ar for 20 h. The reaction was quenched by the addition of water. This solution was washed with dichloromethane three times. The organic solvent was evaporated and the residue was subjected to silica gel column chromatography using toluene to obtain 14.0 mg (16%) of **2b**.

^{1}H-NMR ($CDCl_3$, 500 MHz): δ (ppm) = 9.21 (s, 6H), 8.33 (s, 6H), 2.57 (t, 12H), 1.75–1.69 (m, 12H), 1.42–1.25 (m, 108H), 0.87 (t, 18H). MALDI-TOF mass: m/z = 1717.5 [M^+], calcd for $C_{120}H_{162}BN_6F$ m/z = 1717.3. Visible (dichloromethane) λ_{max}/nm (log ε): 671 (5.04).

2c. In a 100 mL three-necked flask were placed **4** (68 mg, 0.052 mmol), copper iodide (10 mg, 0.053 mmol), $Pd(PPh_3)_4$ (30 mg, 0.026 mmol), and dry dimethylsulfoxide (30 mL), and triethylamine (5.0 mL). Ethynylbenzene (310 mg, 3.03 mmol) was added and the mixture was stirred at 40 °C under Ar for 20 h. Then, hexane is added to the reaction solution, the mixture is filtered, and then a solvent in the filtered solution is removed. The obtained solid was washed with hexane, methanol, acetone, dichloromethane, chloroform, ethyl acetate, 28% aqueous ammonia, and diethyl ether to obtain **2c**: 5.9 mg, 10% yield.

MALDI-TOF mass: m/z = 1164.3 [M^+], calcd for $C_{84}H_{42}BN_6F$ m/z = 1164.4. Visible (dichloromethane) λ_{max}/nm (log ε): 677 (5.01).

2d. In a 100 mL three-necked flask were placed **4** (68 mg, 0.052 mmol), copper iodide (10 mg, 0.053 mmol), $Pd(PPh_3)_4$ (30 mg, 0.026 mmol), and dry dimethylsulfoxide (30 mL), and triethylamine (5.0 mL). *p*-Propylphenylacetylene (440 mg, 3.05 mmol) was added and the mixture was stirred at 40 °C under Ar for 20 h. The reaction solution was subjected to silica gel column chromatography using toluene and evaporated *in vacuo*. The obtained solid was washed with hexane and recrystallized from chloroform to obtain 14.4 mg (20%) of **2d**.

^{1}H-NMR ($CDCl_3$, 500 MHz): δ (ppm) = 9.11 (s, 6H), 8.42 (s, 6H), 7.54 (d, 12H, 5 Hz), 7.15 (m, 12H, 10 Hz), 2.62 (t, 12H), 1.69–1.64 (m, 12H), 0.98 (t, 18H). MALDI-TOF mass: m/z = 1416.6 [M^+], calcd for $C_{102}H_{78}BN_6F$ m/z = 1416.6. Visible (dichloromethane) λ_{max}/nm (log ε): 678 (5.06).

2e. In a 100 mL three-necked flask were placed **4** (68 mg, 0.052 mmol), copper iodide (10 mg, 0.053 mmol), $Pd(PPh_3)_4$ (30 mg, 0.026 mmol), and dry dimethylsulfoxide (30 mL), and triethylamine (5.0 mL). *p*-Ethynylhexylbenzene (570 mg, 3.06 mmol) was added and the mixture was stirred at 40 °C under Ar for 20 h. The reaction was quenched by the addition of water. This solution was washed with dichloromethane three times. The organic solvent was evaporated and the residue was subjected to silica gel column chromatography using toluene to obtain 18.7 mg (22%) of **2e**.

^{1}H-NMR ($CDCl_3$, 500 MHz): δ (ppm) = 9.04 (s, 6H), 8.39 (s, 6H), 7.53 (d, 12H, 10 Hz), 7.11 (d, 12H, 5 Hz), 2.63 (t, 12H), 1.65–1.61 (m, 12H), 1.42–1.25 (m, 36H), 0.92 (t, 18H). MALDI-TOF mass: m/z = 1668.9 [M^+], calcd for $C_{120}H_{114}BN_6F$ m/z = 1668.9. Visible (dichloromethane) λ_{max}/nm (log ε): 678 (5.06).

2f. In a 100 mL three-necked flask were placed **4** (68 mg, 0.052 mmol), copper iodide (10 mg, 0.053 mmol), $Pd(PPh_3)_4$ (30 mg, 0.026 mmol), and dry dimethylsulfoxide (30 mL), and triethylamine (5.0 mL). *p*-Ethynyl(hexyloxy)benzene (620 mg, 3.06 mmol) was added and the mixture was stirred at 40 °C under Ar for 20 h. The reaction was quenched by the addition of water. This solution was washed with dichloromethane three times. The organic solvent was evaporated and the residue was subjected to silica gel column chromatography using toluene to obtain 24.3 mg (27%) of **2f**.

^{1}H-NMR ($CDCl_3$, 500 MHz): δ (ppm) = 8.88 (s, 6H), 8.28 (s, 6H), 7.51 (d, 12H, 10 Hz), 6.81 (d, 12H, 10 Hz), 3.95 (t, 12H), 1.85–1.78 (m, 12H), 1.53–1.45 (m, 12H), 1.43–1.30 (m, 24H), 0.95 (t, 18H). MALDI-TOF mass: m/z = 1765.0 [M^+], calcd for $C_{120}H_{114}BN_6O_6F$ m/z = 1764.9. Visible (dichloromethane) λ_{max}/nm (log ε): 681 (5.05).

2g. In a 100 mL three-necked flask were placed **4** (68 mg, 0.052 mmol), copper iodide (10 mg, 0.053 mmol), $Pd(PPh_3)_4$ (30 mg, 0.026 mmol), and dry dimethylsulfoxide (30 mL), and triethylamine (5.0 mL). 5-Ethynyl-1,2,3-tris(hexyloxy)benzene (1.23 g, 3.05 mmol) was added and the mixture was stirred at 40 °C under Ar for 20 h. The reaction was quenched by the addition of water. This solution was washed with dichloromethane three times. The organic solvent was evaporated and the residue was subjected to silica gel column chromatography using toluene to obtain 15.1 mg (10%) of **2g**.

^{1}H-NMR ($CDCl_3$, 500 MHz): δ (ppm) = 9.33 (s, 6H), 8.51 (s, 6H), 6.58 (s, 12H), 3.98 (t, 12H), 3.89 (t, 24H), 1.82–1.68 (m, 36H), 1.53–1.40 (m, 36H), 1.39–1.27 (m, 72H), 0.97–0.80 (m, 54H). ^{13}C-NMR ($CDCl_3$, 125 MHz): δ (ppm) 153.14, 150.29, 139.54, 132.74, 132.18, 129.34, 124.27, 121.96, 117.28, 110.19,

95.67, 87.08, 73.54, 69.10, 31.78, 31.62, 30.33, 29.33, 25.82, 25.77, 22.71, 22.65, 14.10, 14.05. MALDI-TOF mass: m/z = 2966.0 [M^+], calcd for $C_{192}H_{258}BN_6O_{18}F$ m/z = 2966.0. Visible (dichloromethane) λ_{max}/nm (log ε): 678 (5.06).

5-Bromo-1,2,3-tri(hexyloxy)benzene (13). A 4.9 g portion of 5-bromo-1,2,3-trimethoxybenzene (20 mmol) was dissolved in 100 mL of dichloromethane, and the solution was cooled to −78 °C, followed by the slow addition of 60 mL BBr_3 (1 M in DCM). The mixture was allowed to warm to room temperature over 4 h and stirred for 60 h. The reaction was quenched by ice-water and the mixture was extracted with ethyl acetate (40 mL ×3). The organic layer was concentrated under reduced pressure to afford 4.3 g 5-bromo-1,2,3-benzenetriol as a white solid, which was directly submitted to the next reaction. This solid was dissolved in 100 mL DMF and the solution was degassed by bubbling argon for 15 min, then 24.0 g K_2CO_3 (173 mmol) was added. The mixture was stirred at room temperature for 10 min, and then 12.8 g 1-bromohexane (77.3 mmol) was added. The mixture was heated to 60 °C for 4 h. After cooling, the reaction was quenched by the addition of ice-water. This solution was washed with ethyl acetate (50 mL ×2). The organic solvent was evaporated and the residue was subjected to silica gel column chromatography (*n*-hexane/DCM = 1 : 1) to obtain 6.2 g (65%) of **13** as a white powder.

^{1}H-NMR ($CDCl_3$, 500 MHz): δ (ppm) = 6.67 (s, 2H), 3.92 (m, 6H), 1.84–1.67 (m, 6H), 1.57–1.23 (m, 18H), 0.94–0.85 (m, 9H). MALDI-TOF mass: m/z = 456.2 [M^+], calcd for $C_{24}H_{41}BrO_3$ m/z = 456.2.

1,2,3-Tri(hexyloxy)-5-[2-(trimethylsilyl)ethynyl]benzene (14). In a 100 mL three-necked flask were placed **13** (5.0 g, 11 mmol), copper iodide (100 mg, 0.53 mmol), $Pd(PPh_3)_4$ (1.5 g, 1.3 mmol), and piperidine (30 mL). Trimethylsilylacetylene (1.53 g, 15.6 mmol) was added and the mixture was stirred at 80 °C under Ar for 12 h. The reaction was quenched by the addition of 20 mL 2 M aqueous ammonium chloride. The mixture was extracted with diethyl ether (100 mL ×3) and dichloromethane (100 mL ×2). The organic solvent was evaporated and the residue was subjected to silica gel column chromatography (*n*-hexane/DCM = 1 : 1) to obtain 5.1 g (98%) of **14**.

^{1}H-NMR ($CDCl_3$, 500 MHz): δ (ppm) = 6.66 (s, 2H), 3.97–3.93 (m, 6H), 1.81–1.69 (m, 6H), 1.49–1.28 (m, 18H), 0.92–0.87 (m, 9H). MALDI-TOF mass: m/z = 497.4 [(M + Na)$^+$], calcd for $C_{29}H_{50}O_3SiNa$ m/z = 497.3.

5-Ethynyl-1,2,3-tri(hexyloxy)benzene (15). Compound **2** (4.0 g, 8.4 mmol) was dissolved in 40 mL dichloromethane and 40 mL of methanol, and then 3.50 g potassium carbonate (25.4 mmol) was added. The mixture was stirred for 4 h at room temperature. The reaction was quenched by the addition of 20 mL water. This solution was washed with DCM (100 mL ×2). The organic layer was concentrated under reduced pressure and the residue was purified by silica gel column chromatography (*n*-hexane/DCM = 4 : 1) to give 2.9 g of title product **15** (86%). ^{1}H NMR spectrum was identical to that reported in the literature.[32]

^{1}H-NMR ($CDCl_3$, 500 MHz): δ (ppm) = 6.69 (s, 2H), 3.98–3.93 (m, 6H), 2.99 (s, 1H), 1.81–1.70 (m, 6H), 1.49–1.30 (m, 18H), 0.92–0.88 (m, 9H). MALDI-TOF mass: m/z = 425.3 [(M + Na)$^+$], calcd for $C_{26}H_{42}O_3Na$ m/z = 425.3.

Conclusions

Chloroboron(III) and fluoroboron(III) hexaethynyl-subnaphthalocyanines were prepared by Sonogashira coupling. The B–F derivatives showed higher melting points and lower solubilities than the corresponding B–Cl derivatives. XRD, POM, visible spectroscopic studies indicated that the B–F derivatives were packed in the hexagonal columnar structure, while the B–Cl derivatives were poorly crystalline. The B–F derivatives with hexylphenyl or hexyloxyphenyl groups showed mesophase at 180 °C. We demonstrated that design of the peripheral substituents and the axial halogen is efficient strategy to control molecular packing of highly polar subnaphthalocyanines.

Conflicts of interest

There are no conflicts to declare.

Acknowledgements

We thank Drs Toshinobu Ohno and Yo Shimizu for valuable discussions. We also thank Koji Ohoka for his help in high resolution mass spectroscopic studies.

Notes and references

1 (*a*) G. E. Morse and T. P. Bender, *ACS Appl. Mater. Interfaces*, 2012, **4**, 5055; G. de la Torre, G. Bottari and T. Torres, *Adv. Energy Mater.*, 2017, **7**, 1601700. (*b*) K. Cnops, G. Zango, J. Genoe, P. Heremans, M. V. Martinez-Diaz, T. Torres and D. Cheyns, *J. Am. Chem. Soc.*, 2015, **137**, 8991.

2 D. Hohnholz, S. Steinbrecher and M. Hanack, *J. Mol. Struct.*, 2000, **521**, 231.

3 (*a*) C. Piechocki, J. Simon, A. Skoulios, D. Guillon and P. Weber, *J. Am. Chem. Soc.*, 1982, **104**, 5245; (*b*) B. A. Gregg, M. A. Fox and A. J. Bard, *J. Am. Chem. Soc.*, 1989, **111**, 3024; (*c*) B. A. Gregg, M. A. Fox and A. J. Bard, *J. Phys. Chem.*, 1990, **94**, 1586; (*d*) P. G. Schouten, J. M. Warman, M. P. de Haas, M. A. Fox and H.-L. Pan, *Nature*, 1991, **353**, 736; (*e*) K. Hatsusaka, K. Ohta, I. Yamamoto and H. Shirai, *J. Mater. Chem.*, 2001, **11**, 423.

4 (*a*) H. E. Katz, Z. Bao and S. L. Gilat, *Acc. Chem. Res.*, 2001, **34**, 359; (*b*) C. D. Sheraw, T. N. Jackson, D. L. Eaton and J. E. Anthony, *Adv. Mater.*, 2003, **15**, 2009; (*c*) C. R. Newman, C. D. Frisbie, D. A. da Silva Filho, J.-L. Bredas, P. C. Ewbank and K. R. Mann, *Chem. Mater.*, 2004, **16**, 4436; (*d*) S. Sergeyev, W. Pisula and Y. H. Geerts, *Chem. Soc. Rev.*, 2007, **36**, 1902; (*e*) Q. Ye, J. Chang, K.-W. Huang and C. Chi, *Org. Lett.*, 2011, **13**, 5960.

5 P. G. Schouten, J. M. Warman, M. P. de Haas, C. F. van Nostrum, G. H. Gelinck, R. J. M. Nolte, M. J. Copyn, J. W. Zwikker, M. K. Engel, M. Hanack, Y. H. Chang and W. T. Ford, *J. Am. Chem. Soc.*, 1994, **116**, 6880.

6 H. Kietaibl, *Monatsh. Chem.*, 1974, **105**, 405.

7 C. G. Claessens, D. Gonzalez-Rodriguez, M. S. Rodriguez-Morgade, A. Medina and T. Torres, *Chem. Rev.*, 2014, **114**, 2192.
8 B. Verreet, S. Schols, D. Cheyns, B. P. Rand, H. Gommans, T. Aernouts, P. Heremans and J. Genoe, *J. Mater. Chem.*, 2009, **19**, 5295.
9 A. M. van der Craats and J. M. Warman, *Adv. Mater.*, 2001, **13**, 130.
10 J. Guilleme, J. Arago, E. Orti, E. Cavero, T. Sierra, J. Ortega, C. L. Folcia, J. Etxebarria, D. Gonzalez-Rodriguez and T. Torres, *J. Mater. Chem. C*, 2015, **3**, 985.
11 (*a*) K. L. Mutolo, E. I. Mayo, B. P. Rand, S. R. Forrest and M. E. Thompson, *J. Am. Chem. Soc.*, 2006, **128**, 8108; (*b*) H. Gommans, T. Aernouts, B. Verreet, P. Heremans, A. Medina, C. G. Claessens and T. Torres, *Adv. Funct. Mater.*, 2009, **19**, 3435; (*c*) H. Gommans, T. Aernouts, B. Verreet, P. Heremans, A. Medina, C. G. Claessens and T. Torres, *Adv. Funct. Mater.*, 2009, **19**, 3435; (*d*) B. Ma, C. H. Woo, Y. Miyamoto and J. M. J. Frechet, *Chem. Mater.*, 2009, **21**, 1413.
12 (*a*) Y. Takao, T. Masuoka, K. Yamamoto, T. Mizutani, F. Matsumoto, K. Moriwaki, K. Hida, T. Iwai, T. Ito, T. Mizuno and T. Ohno, *Tetrahedron Lett.*, 2014, **55**, 4564; (*b*) K. Yamamoto, A. Takagi, M. Hada, R. Taniwaki, T. Mizutani, Y. Kimura, Y. Takao, K. Moriwaki, F. Matsumoto, T. Ito, T. Iwai, K. Hida, T. Mizuno and T. Ohno, *Tetrahedron*, 2016, **72**, 4918.
13 D. S. Terekhov, K. J. M. Nolan, C. R. McArthur and C. C. Leznoff, *J. Org. Chem.*, 1996, **61**, 3034.
14 J. D. Dang, D. S. Josey, A. J. Lough, Y. Li, A. Sifate, Z.-H. Luc and T. P. Bender, *J. Mater. Chem. A*, 2016, **4**, 9566.
15 K. Sonogashira, Y. Tohda and N. Hagihara, *Tetrahedron Lett.*, 1975, 4467.
16 J. Guilleme, D. Gonzalez-Rodriguez and T. Torres, *Angew. Chem., Int. Ed.*, 2011, **50**, 3506.
17 D. Velasco, V. Jankauskas, J. Stumbraite, J. V. Grazulevicius and V. Getautis, *Synth. Met.*, 2009, **159**, 654.
18 M. V. Fulford, D. Jaidka, A. S. Paton, G. E. Morse, E. R. L. Brisson, A. J. Lough and T. P. Bender, *J. Chem. Eng. Data*, 2012, **57**, 2756.
19 G. Martin, G. Rojo, F. Agullo-Lopez, V. R. Ferro, J. M. G. de la Vega, M. V. Martinez-Diaz, T. Torres, I. Ledoux and J. Zyss, *J. Phys. Chem. B*, 2002, **106**, 13139.
20 M. Kasha, H. R. Rawls, M. Ashraf and A. El-Bayoumi, *Pure Appl. Chem.*, 1965, **11**, 371.
21 J. M. Kroon, R. B. M. Koehorst, M. van Dijk, G. M. Sanders and E. J. R. Sudholter, *J. Mater. Chem.*, 1997, **7**, 615.
22 C. Colomban, E. V. Kudrik, V. Briois, J. C. Shwarbrick, A. B. Sorokin and P. Afanasiev, *Inorg. Chem.*, 2014, **53**, 11517.
23 B. Koksoy, O. Soyer, E. B. Orman, A. R. Ozkaya and M. Bulut, *Dyes Pigm.*, 2015, **118**, 166.
24 N. Kobayashi, T. Ishizaki, K. Ishii and H. Konami, *J. Am. Chem. Soc.*, 1999, **121**, 9096.
25 S. Nonell, N. Rubio, B. del Rey and T. Torres, *J. Chem. Soc., Perkin Trans. 2*, 2000, 1091.
26 A. Concellon, M. Marcos, P. Romero, J. L. Serrano, R. Termine and A. Golemme, *Angew. Chem., Int. Ed.*, 2017, **56**, 1259.
27 S. H. Kang, Y.-S. Kang, W.-C. Zin, G. Olbrechts, K. Wostyn, K. Clays, A. Persoons and K. Kim, *Chem. Commun.*, 1999, 1661.
28 (*a*) M. S. Rodriguez-Morgade, C. G. Claessens, A. Medina, D. Gonzalez-Rodriguez, E. Gutierrez-Puebla, A. Monge, I. Alkorta, J. Elguero and T. Torres, *Chem.–Eur. J.*, 2008, **14**, 1342; (*b*) J. Guilleme, M. J. Mayoral, J. Calbo, J. Arago, P. M. Viruela, E. Orti, T. Torres and D. Gonzalez-Rodriguez, *Angew. Chem., Int. Ed.*, 2015, **54**, 2543.
29 M. Mantina, A. C. Chamberlin, R. Valero, C. J. Cramer and D. G. Truhlar, *J. Phys. Chem. A*, 2009, **113**, 5806.
30 A. Bondi, *J. Phys. Chem.*, 1964, **68**, 441.
31 M. J. Frisch, G. W. Trucks, H. B. Schlegel, G. E. Scuseria, M. A. Robb, J. R. Cheeseman, G. Scalmani, V. Barone, B. Mennucci, G. A. Petersson, H. Nakatsuji, M. Caricato, X. Li, H. P. Hratchian, A. F. Izmaylov, J. Bloino, G. Zheng, J. L. Sonnenberg, M. Hada, M. Ehara, K. Toyota, R. Fukuda, J. Hasegawa, M. Ishida, T. Nakajima, Y. Honda, O. Kitao, H. Nakai, T. Vreven, J. J. A. Montgomery, J. E. Peralta, F. Ogliaro, M. Bearpark, J. J. Heyd, E. Brothers, K. N. Kudin, V. N. Staroverov, R. Kobayashi, J. Normand, K. Raghavachari, A. Rendell, J. C. Burant, S. S. Iyengar, J. Tomasi, M. Cossi, N. Rega, J. M. Millam, M. Klene, J. E. Knox, J. B. Cross, V. Bakken, C. Adamo, J. Jaramillo, R. Gomperts, R. E. Stratmann, O. Yazyev, A. J. Austin, R. Cammi, C. Pomelli, J. W. Ochterski, R. L. Martin, K. Morokuma, V. G. Zakrzewski, G. A. Voth, P. Salvador, J. J. Dannenberg, S. Dapprich, A. D. Daniels, O. Farkas, J. B. Foresman, J. V. Ortiz, J. Cioslowski, and D. J. Fox, in *Gaussian 09, Revision A.02*, 2009; M. J. Frisch, G. W. Trucks, H. B. Schlegel, G. E. Scuseria, M. A. Robb, J. R. Cheeseman, G. Scalmani, V. Barone, B. Mennucci, G. A. Petersson, H. Nakatsuji, M. Caricato, X. Li, H. P. Hratchian, A. F. Izmaylov, J. Bloino, G. Zheng, J. L. Sonnenberg, M. Hada, M. Ehara, K. Toyota, R. Fukuda, J. Hasegawa, M. Ishida, T. Nakajima, Y. Honda, O. Kitao, H. Nakai, T. Vreven, J. A. Montgomery, J. E. Peralta, F. Ogliaro, M. Bearpark, J. J. Heyd, E. Brothers, K. N. Kudin, V. N. Staroverov, R. Kobayashi, J. Normand, K. Raghavachari, A. Rendell, J. C. Burant, S. S. Iyengar, J. Tomasi, M. Cossi, N. Rega, J. M. Millam, M. Klene, J. E. Knox, J. B. Cross, V. Bakken, C. Adamo, J. Jaramillo, R. Gomperts, R. E. Stratmann, O. Yazyev, A. J. Austin, R. Cammi, C. Pomelli, J. W. Ochterski, R. L. Martin, K. Morokuma, V. G. Zakrzewski, G. A. Voth, P. Salvador, J. J. Dannenberg, S. Dapprich, A. D. Daniels, O. Farkas, J. B. Foresman, J. V. Ortiz, J. Cioslowski and D. J. Fox, Gaussian, Inc., Wallingford CT, 2009.
32 Y. Long, H. Chen, Y. Yang, H. Wang, Y. Yang, N. Li, K. Li, J. Pei and F. Liu, *Macromolecules*, 2009, **42**, 6501.